Chemical Physics 179 (1994) 583–593
North-Holland

Reaction dynamics of collisionally activated ammonia cations

Bernard Leyh [1,*] and Antuan Hoxha
Département de Chimie, Université de Liège, B-4000 Sart-Tilman (Liège 1), Belgium

Received 26 July 1993

In the framework of a research project on the collisional mechanisms involved in tandem mass spectrometry, the collisional activation processes of NH_3^+ with different target gases have been investigated. The experiments have been performed on an upgraded AEI-MS9 sector instrument equipped with two collision cells and include daughter ion spectra, ion kinetic energy spectra, determination of kinetic energy release distributions (KERD) and appearance energy measurements. We have shown that collisionally activated dissociation (CAD) of NH_3^+ into $NH^+ + [H, H]$ depends on the internal energy of NH_3^+. This internal energy effect is also observed for the $NH_2^+ + H$ channel, when Xe is the target gas; with He, such an effect could not be detected. The analysis of the KERD shows that production of NH_2^+ upon CAD takes place from the NH_3^+ ground electronic state by rotational predissociation; two components are observed, one which corresponds to a near-threshold process (mean kinetic energy release $\langle T \rangle = 0.13$ eV), and one characterized by $\langle T \rangle = 0.56$ eV corresponding to an excess energy of 2.1 eV above the dissociation threshold. NH^+ fragments can be formed by two processes: the first one occurs at threshold and leads to $NH^+(X\,^2\Pi) + H_2(X\,^1\Sigma_g^+)$; the second one is characterized by large KER values (up to 7 eV) and leads to either electronically excited NH^+ or dissociation of H_2.

1. Introduction

Collisional activation (CA) is certainly the most widely used activation technique in tandem mass spectrometry [1,2]. Despite the wealth of applications of this method, its basic physicochemical mechanisms are still poorly understood, particularly in the case of polyatomic molecules. In this paper, we are interested in the high energy collision regime (a few keV) and will consider the two following questions:

(i) How does the distribution of internal energy deposited in the projectile ion depend on the nature of the target gas?

(ii) Does the amount of internal energy of the projectile ion before the collision influence the collision and dissociation dynamics?

We have investigated these questions in the case of NH_3^+ resulting from electroionization of ammonia. Because of its relevance for important problems related, e.g., to atmospheric physics and chemistry, to plasma physics, to laser chemistry, the ammonia cation has been one of the most studied ions, both experimentally [3–21] and theoretically [22–29]. Nearly all available experimental methods have been used: charge exchange [3], dissociative electroionization [5–11], dissociative photoionization [12], fluorescence [9,10,13], photoion–photoelectron coincidence spectroscopy [4,15–17], dissociative electroionization coupled with translational energy spectroscopy [18–20], study of metastable fragmentation [14]. Besides its importance in tandem mass spectrometry, collisional activation also provides complementary fundamental information on the dissociation dynamics of an ion because of the possibility of modulating the internal energy distribution by changing the target gas.

The lowest dissociation channel, $NH_2^+ + H$, has an onset of 15.76 eV [5,18] with respect to the ground state of neutral ammonia: this threshold is therefore located within the $\tilde{A}\,^2E$ state of NH_3^+. According to ref. [26], production of these fragments results from a rapid (10^{-14}–10^{-13} s) internal conversion from the $\tilde{A}$ to the $\tilde{X}$ state, via a conical intersection. This first step is then followed by rotational predissociation

[1] Chercheur qualifié du Fonds National de la Recherche Scientifique (Belgium).

* Corresponding author.

0301-0104/94/$ 07.00 © 1994 Elsevier Science B.V. All rights reserved.
SSDI 0301-0104(93)E0399-G

[15,16]. At threshold this process occurs via tunneling through the centrifugal barrier and leads to a microcanonical rate constant in the metastable window ($k \approx 10^6\ s^{-1}$) [14].

The threshold for the production of the $NH^+(X\,^2\Pi) + H_2(X\,^1\Sigma_g^+)$ fragments is about 17 eV [5,18]. Following electron impact, a significant ion current is detected only at energies higher than 18 eV. This asymptote is correlated with the $\tilde{A}\,^2E$ state of NH_3^+. More energetic processes leading to electronically excited NH^+ and/or dissociation of H_2 have also been observed [6,9,10,12,18] and will be shown to be relevant to collisionally activated dissociation (CAD) of NH_3^+. The relevant electronic states and dissociation channels are summarized in fig. 1.

2. Experimental

The experiments have been performed on a double-focusing AEI-MS9 mass spectrometer (EB geometry) recently modified by the installation of a collision cell in both the first (between the source exit slit and the electrostatic analyzer) and the second (between the electrostatic analyzer and the magnet) field-free regions. Three kinds of spectra have been measured.

(i) Daughter ion spectra resulting from dissociations taking place in the collision cell located in the first field-free region have been recorded using the technique of linked scanning at constant B/E [30]; the magnetic field is then controlled via a Hall probe.

(ii) Ion kinetic energy spectra for dissociations taking place in the first field-free region have been recorded by the accelerating voltage scan technique [31]. In such spectra, the source high voltage V_{acc}, which determines the ion kinetic energy in the laboratory frame ($E_k = zeV_{acc}$), is scanned upwards to allow transmitting fragment ions resulting from dissociations in the first field-free region. Examples of such spectra are shown in fig. 2.

(iii) Appearance energy spectra have been measured by the vanishing current method [32,33]; the energy scale has been calibrated by measuring the appearance energy of rare gases under identical experimental conditions.

The experimental conditions were as follows: trap current 30 μA, electron energy 70 eV. For the linked scans at constant B/E, the accelerating voltage was set at 8000 V. The β-slit (energy resolving slit) was closed to reach an energy resolution of 5 eV in the ion

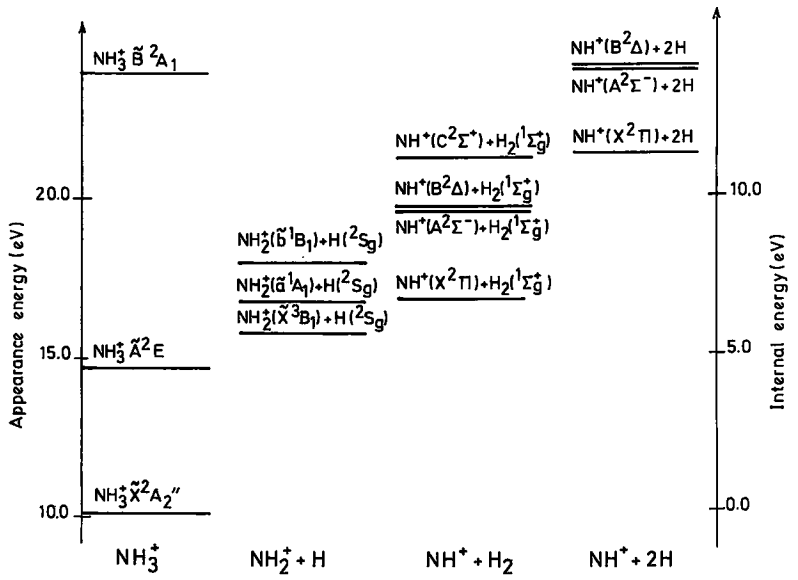

Fig. 1. Energetics of the electronic states and dissociation channels relevant for the collisionally activated dissociation of NH_3^+.

kinetic energy spectra. This energy resolution in the laboratory frame corresponds to a resolution of 4 meV for the kinetic energy released on the $NH_2^+ + H$ fragments measured in the molecular centre of mass frame. NH_3 from Air Products (purity > 99.999%; $H_2O < 3$ ppm) was used without further purification. All rare gas targets had a purity better than 99.99%. Benzene had a purity of 99.7%. The interferences due to OH^+ and O^+ have been shown to be negligible: $I(OH^+)/I(NH_3^+) = 0.1\%$; $I(O^+)/I(NH_2^+) < 0.02\%$ at a typical source pressure of 1.2×10^{-6} Torr (measured about 15 cm from the ionization chamber). All collisional experiments have been performed with a low target gas pressure (transmittance of the primary beam $\geqslant 90\%$) to ensure single collision conditions [34,35].

3. Results

3.1. Daughter ion spectra

Daughter ion spectra of collisionally activated NH_3^+ ions have been recorded in the $m/z = 13$ to 17 range. Collisions take place in the cell located in the first field-free region. The data are presented in table 1. All intensity data are obtained by measuring peak areas rather than peak heights. The relative collision energy (E_{rel}) in the fourth column of table 1 is related to the translational energy in the laboratory frame (E_{lab}) by the relation:

$$E_{rel} = E_{lab} m_G / (m_G + m_P) ,$$

where m_G is the mass of the neutral target and m_P is the mass of the ionic projectile.

The metastable loss of H can also take place, but is characterized by a much smaller kinetic energy release on the fragments (in the meV range [14]) than the CAD process (see section 3.2 below). On the other hand, measurements of the variation of the NH^+ signal, without gas in the collision cell, as a function of the source pressure show that the $NH_3^+ \rightarrow NH^+ + [H, H]$ process is not a real metastable process, but is induced by the negligible flow of gas from the source to the first field-free region. This is confirmed by appearance energy measurements.

3.2. Ion kinetic energy spectra

Fig. 2 shows one example of the ion kinetic energy spectra obtained by the accelerating voltage scan technique for the $NH_3^+ \rightarrow NH_2^+ + H$ and $NH_3^+ \rightarrow NH^+ + [H, H]$ CAD processes. The target gas was He at a precursor beam transmittance of 90%. The [H, H] notation includes both formation of H_2 and 2H. The kinetic energy release (KER) corresponding to the peak width at half height ($T_{0.5}$) has been calculated for the different target gases used. These values are displayed in the second and fifth columns of table 2.

To reach a more detailed understanding of these

Table 1
Branching ratios, internal energies and collisional energy transfer in collisional activation of fast NH_3^+ cations

Target gas	Ionization energy (eV)	Collision energy (keV)		$I(NH^+)/I(NH_2^+)$ (%)	$I(N^+)/I(NH_2^+)$ (%)	$\langle E_{int} \rangle$ (eV)	Energy loss [a] (eV)
		laboratory frame	relative				
He	24.59	8	1.5	4.9	0.8	8.5	3.5
Ar	15.76	8	5.6	3.7	0.4	8.4	2.6
Ar	15.76	2	1.4	1.5	0.1	8.0	
Xe	12.13	8	7.1	2.0	< 0.1	8.1	0.7
C_6H_6	9.25	8	6.6	2.7	0.3	8.2	2.2
metastable		8		0.3 [b]	not detected		

[a] These values correspond to the translational energy loss of NH_3^+ ions resulting from a collision with a target gas atom or molecule and leading to the $NH_2^+ + H$ fragments.

[b] This $NH_3^+ \rightarrow NH^+ + [H, H]$ process is not a real metastable process; it is induced by the small amount of gas flowing from the source to the first field-free region (see discussion in the text).

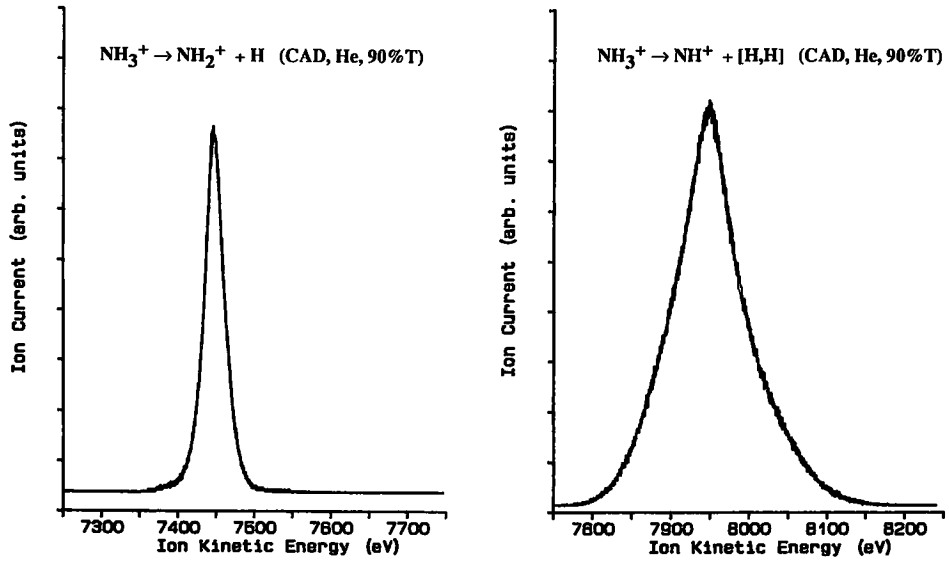

Fig. 2. Ion kinetic energy spectrum for the $NH_3^+ \rightarrow NH_2^+ + H$ (left) and $NH_3^+ \rightarrow NH^+ + [H, H]$ (right) collisionally activated dissociations. Target gas: He. Precursor beam transmittance: 90%. CAD takes place in the collision cell located in the first field-free region of the mass spectrometer. These ion kinetic energy spectra were recorded using the accelerating voltage scan technique.

Table 2
Kinetic energy release corresponding to the peak width at half height ($T_{0.5}$) and average kinetic energy release $\langle T \rangle$ for the loss of H and [H, H] from collisionally activated NH_3^+ cations. All values are in eV. The translational energy of the fragment ions (laboratory frame) is equal to 7 keV

Target gas	$NH_3^+ \rightarrow NH_2^+ + H$			$NH_3^+ \rightarrow NH^+ + [H, H]$		
	$T_{0.5}$	$\langle T \rangle$	$\langle T \rangle / T_{0.5}$	$T_{0.5}$	$\langle T \rangle$	$\langle T \rangle / T_{0.5}$
He	0.14	0.38	2.7	0.75	1.83	2.4
Ar	0.13	0.33	2.5	0.46	1.39	3.0
Xe	0.10	0.20	2.0	0.31	1.04	3.4
C_6H_6	0.11	0.31	2.8	0.53	1.41	2.7

processes, we have analyzed the ion kinetic energy spectra by the Holmes–Osborne procedure [36] to obtain the corresponding kinetic energy release distributions $n(T)$ (KERD). Such distributions contain valuable information concerning the partitioning of the excess energy (above the thermochemical threshold) between internal degrees of freedom of the fragments and the reaction coordinate. For the analysis of ion kinetic energy spectra obtained under CAD conditions, one has to be aware of the spread of the parent ion internal energy reached upon collision: this leads to a tail on the high acceleration voltage side of the peak, due to the conversion, upon collision, of translational energy into internal energy. Kim and Kim [37] have developed a method to extract KERD curves for CAD processes while taking this asymmetry into account. In the cases studied here, however, no significant asymmetry has been observed: the KERD obtained by analyzing both halves of the ion kinetic energy spectrum are very similar. This means that the distribution of translational energy losses is narrower than the width due to the release of kinetic energy. Fig. 3 shows the KERDs obtained with different target gases for the $NH_3^+ \rightarrow NH_2^+ + H$ dissociation and fig. 4 shows the data for $NH_3^+ \rightarrow NH^+ + [H, H]$ reaction. The KERDs shown result from the analysis

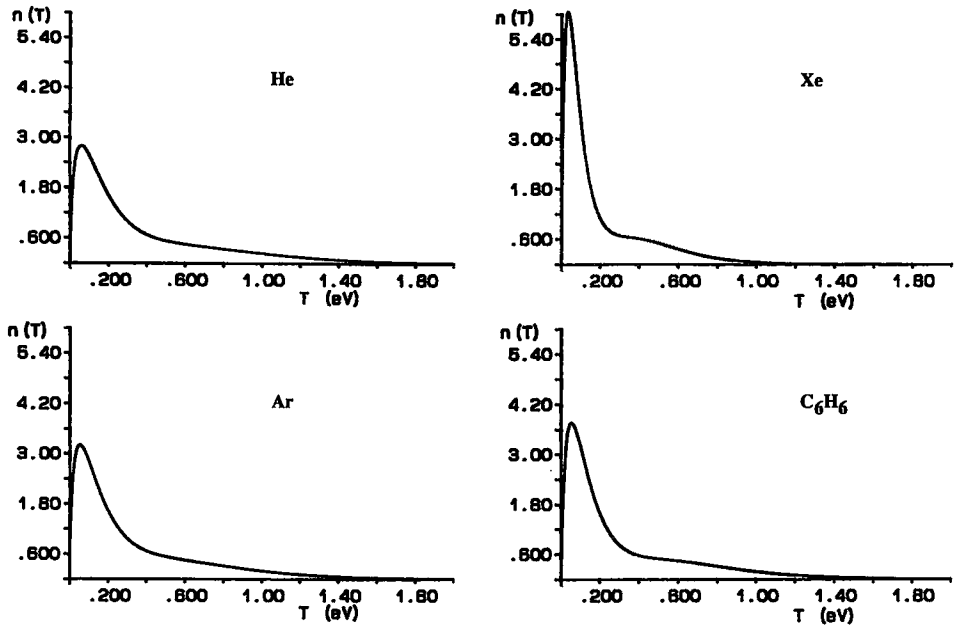

Fig. 3. Kinetic energy release distribution for the $NH_3^+ \rightarrow NH_2^+ + H$ collisionally activated dissociation. The target gases used are mentioned in the figure. Precursor beam transmittance: 90%. The kinetic energy release distributions have been obtained from the ion kinetic energy spectra by the Holmes–Osborne procedure.

of the low acceleration voltage half of the dissociation peak: this part of the spectrum is less likely to be perturbed by the collisional energy transfer to NH_3^+. In addition, the average kinetic energy release values, $\langle T \rangle$, are mentioned in the third and sixth columns of table 2.

3.3. Appearance energy spectra

Our aim was to obtain information about the possible role of internal energy of the precursor ion in the CAD process. To reach this goal, we used a method similar to that used by Leyh and Wankenne [38] for charge reversal processes. The intensity of both the parent (NH_3^+) and the fragment ion (NH_2^+, e.g.) were recorded as a function of the energy of the ionizing electrons. The ratio of these intensities is then calculated. If all parent ions are in the ground state when they reach the collision cell of the first field-free region, both appearance energy curves have the same curvature and the intensity ratio is constant. If part of the parent ion beam consists of excited ions, and if the cross section for CAD is different in the ground and in the excited state, the intensity ratio is characterized by a change of slope at the appearance energy corresponding to the excited state. Figs. 5 and 6 show such curves for the loss of H and the loss of [H, H] from NH_3^+ with He and Xe as target gases. A sharp increase of the CAD relative cross section is clearly seen at 14.6 ± 0.8 eV for NH^+ with He and Xe and for NH_2^+ with Xe. Let us note that it is impractical to record such intensity ratios down to the NH_3^+ threshold where the ion currents become very small resulting in unstable values of their ratio.

4. Discussion

4.1. Energy deposition as a function of the target gas

The ratio of fragment ion abundances in a mass spectrum results from the convolution of the breakdown diagram with the internal energy distribution of the parent ion. Starting from the observed branching ratios (table 1) and from the available break-

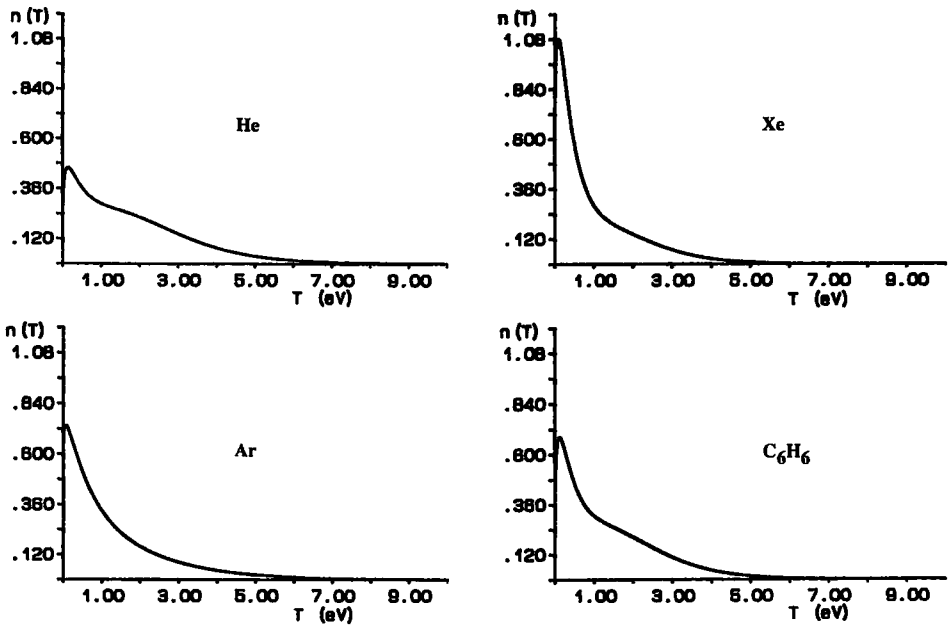

Fig. 4. Kinetic energy release distribution for the $NH_3^+ \rightarrow NH^+ + [H, H]$ collisionally activated dissociation. The target gases used are mentioned in the figure. Precursor beam transmittance: 90%. The kinetic energy release distributions have been obtained from the ion kinetic energy spectra by the Holmes–Osborne procedure.

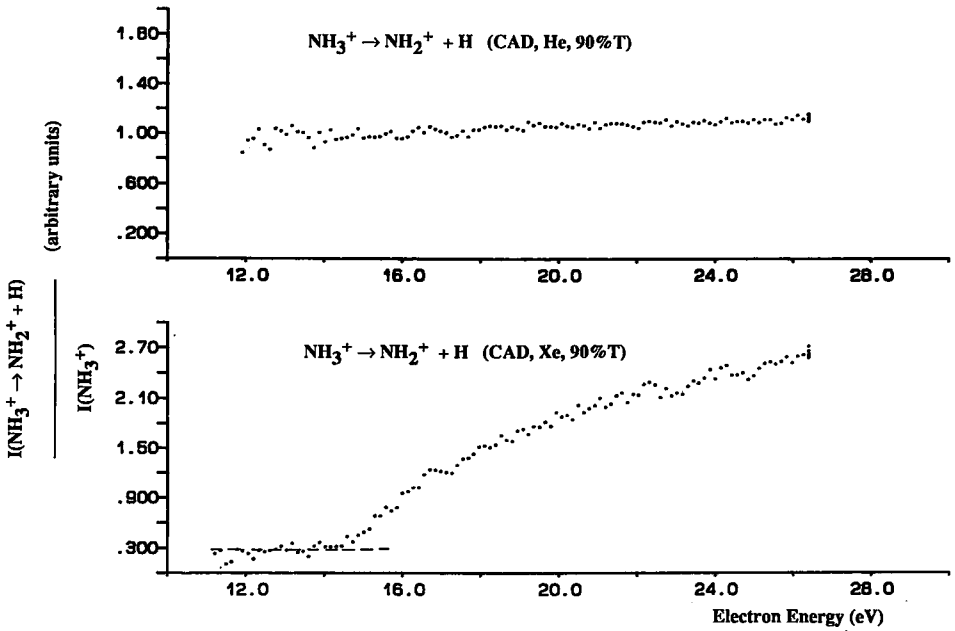

Fig. 5. Ratio of the appearance energy curves (versus energy of the ionizing electrons) for the $NH_3^+ \rightarrow NH_2^+ + H$ collisionally activated dissociation and for the precursor NH_3^+ ion. Target gases: He (top) and Xe (bottom). Precursor beam transmittance: 90%.

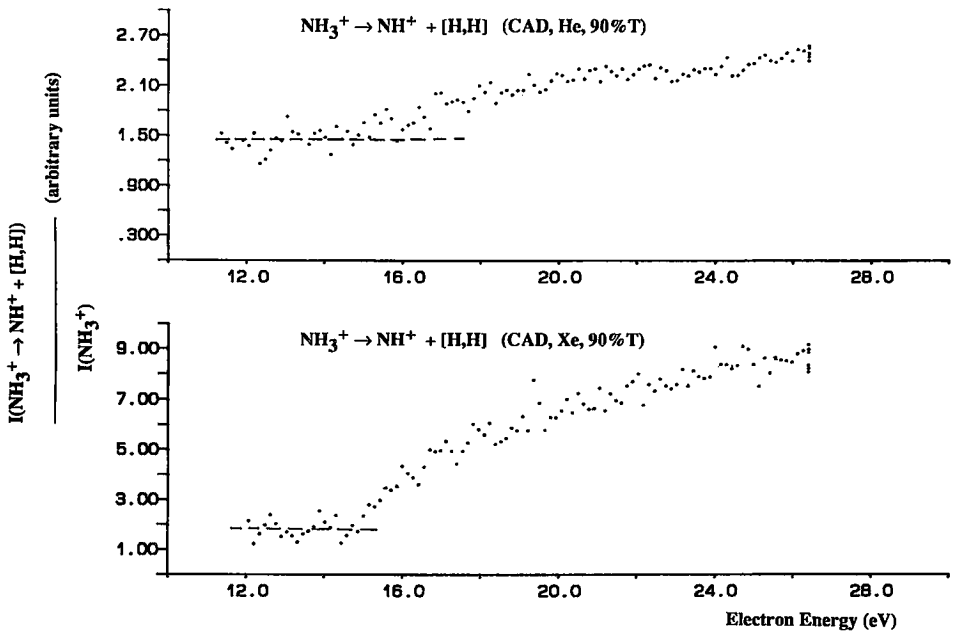

Fig. 6. Ratio of the appearance energy curves (versus energy of the ionizing electrons) for the $NH_3^+ \rightarrow NH^+ + [H, H]$ collisionally activated dissociation and for the precursor NH_3^+ ion. Target gases: He (top) and Xe (bottom). Precursor beam transmittance: 90%.

down diagrams [3,17], it is possible to extract a histogram of the NH_3^+ internal energy distribution excited by the collision process. The average internal energy, $\langle E_{int} \rangle$ can then be calculated from this distribution. It must be stressed that this average internal energy concerns only that part of the NH_3^+ ions which have, after collision, enough energy to dissociate; the ions to which a too small amount of energy has been transferred and which do not dissociate are not considered in the calculation of $\langle E_{int} \rangle$.

The seventh column of table 1 gives the NH_3^+ average internal energies, measured with respect to the ionic ground state, for the different target gases used in this work. The general trend observed, He > Ar > C_6H_6 > Xe ≫ MI, follows, as far as the rare gases are concerned, the ionization energy series [39]. At a given translational energy in the laboratory frame, the variations of $\langle E_{int} \rangle$ between the different target gases are, surprisingly, relatively small: 0.4 eV between Xe and He. The important parameter is, however, the collision energy associated with the relative motion of the target and the projectile: this energy, given in the fourth column of table 1, increases with the target mass, i.e., from He to Xe and varies therefore in opposite direction of the ionization energy series. When He and Ar are used at approximately the same collision energy (1.4–1.5 keV), the difference of $\langle E_{int} \rangle$ is equal to 0.5 eV, whereas this difference drops to 0.1 eV when the collisions take place, for both target gases, at the same translational energy in the laboratory frame (8 keV). C_6H_6 does not follow the ionization energy series. The strong anisotropy of its molecular field as well as the possibility of interactions with its internal degrees of freedom should be considered in detail to account for our experimental data. In a related work to be published [40] on the single electron capture by ammonia dications, we will show that, for molecular targets, the consideration of the lowest ionization energy is not a sufficient criterion and that excitation of the target gas can be significant.

4.2. Influence of the precursor internal energy prior to collisional activation

As mentioned in section 3.3, one observes a sharp increase in the ratio of the appearance energy curves for the loss of H (target gas = Xe) and for the loss of [H, H] (target gas = Xe and He) at 14.6 ± 0.8 eV

(with respect to the neutral ground state) (figs. 5 and 6). This energy is equal, within experimental error, to the onset of the second band of the photoelectron spectrum of NH_3 (14.76 eV), corresponding to the $\tilde{A}\,^2E$ ionic state. This means that the production of NH^+ and NH_2^+ is strongly favoured when the parent ion already possesses an internal energy of about 4.5 eV, prior to the collisional event.

Dujardin and Leach [13] have not succeeded in detecting fluorescence from the $\tilde{A}\,^2E$ state of NH_3^+ and explained their observation by an ultrafast (10^{-14}–10^{-13} s) internal conversion brought about by a conical intersection between the $\tilde{X}\,^2A_2''$ and the $^2A''$ Jahn–Teller component of the $\tilde{A}\,^2E$ state [23,26]. This process leads to the population of highly excited vibrational levels of the electronic ground state. Such states can only relax via infrared fluorescence, which is typically a slow process ($k \approx 10^5$ s^{-1}). It follows that our NH_3^+ ion beam contains long-lived highly excited vibrational states which survive for a few μs. Collisional activation of such already excited states has a much more favourable cross section than collisional activation of cool ions. These results can be correlated with other experimental observations.

(i) By varying the pressure in a CI source, van Koppen et al. [21] could influence the amount of internal energy of the NH_3^+ ions. This was shown to perturb strongly the CAD fragment ion distribution, with He as the target gas.

(ii) Mauclaire et al. [41] have given an upper limit of ≈ 1 ms for the lifetime of highly excited vibrational levels of the bending mode of the ammonia cation. They also mention that the symmetry stretching modes might be very long-lived (10–20 ms).

We have also measured the most probable translational energy loss for collisionally activated ions dissociating in the $NH_2^+ + H$ channel. The energy loss was obtained as the difference between the position of the maximum of the dissociation signal in the accelerating voltage scan with a target gas in the collisional cell (CAD conditions) and without target gas (metastable dissociation conditions). In these experiments, the fragment translational energy was set at 7 keV. This energy loss is equal to the collisional energy uptake by NH_3^+. It is important to mention that, among all ammonia cations, we sample here only those cations which dissociate by the loss of H. The data are collected in the last column of table 1. Three conclusions can be drawn from these experiments.

(i) The energy loss series observed is consistent with our other data concerning the amount of energy deposited into the precursor ion.

(ii) With Xe as the target gas, the most probable energy transferred to NH_3^+ is too small to induce dissociation. It is therefore totally logical that ions which are already vibrationally excited have a much higher CAD cross section (fig. 5).

(iii) Even with He as the target gas, at the most probable energy loss, some of the parent internal energy has to be used. This excitation energy would, however, correspond to the first band of the photoelectron spectrum and is too close to the NH_3^+ appearance energy to be detected with sufficient accuracy by the method described in section 3.3. We may furthermore expect that, due to the distribution of energy losses around an already much larger average value than in the Xe case, the change of slope will be much less pronounced with the He target, as is indeed observed for the loss of [H, H] (compare the top and bottom parts of fig. 6).

4.3. Partition of the excess energy

The KERD curves for the collisionally activated $NH_3^+ \rightarrow NH_2^+ + H$ reaction (fig. 3) show two regimes, a first one characterized by KER values lower than 0.2 eV and a second one extending up to nearly 2 eV. By comparing these curves with those of Powis (fig. 4 of ref. [15]) obtained at selected internal energies (PIPECO spectroscopy), it becomes clear that these two regimes must be correlated with different internal energy domains. According to the work of Powis [15,16], the internal energy corresponding to the low KER regime is then close to the dissociation asymptote. In order to analyze our data more accurately, we assumed that the observed CAD process results from two independent processes, each characterized by a Gaussian peak in the ion kinetic energy spectrum. We have then fitted the experimental peak to a linear combination of two Gaussian curves and have calculated the KERD curves from this fit (i) for the entire peak and (ii) for each component separately. The result is shown in fig. 7 for the He case. The average KER value, $\langle T \rangle$, for the first process is equal to 0.13 eV: this corresponds, according to Powis [15], to an average internal energy of 6 eV. The second process

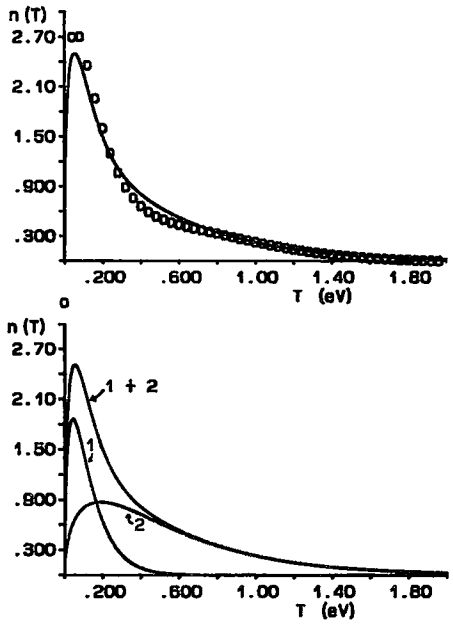

Fig. 7. Kinetic energy release distribution for the $NH_3^+ \rightarrow NH_2^+ + H$ collisionally activated dissociation. Target gas: He. Precursor beam transmittance: 90%. Top: circles: KERD obtained via the Holmes–Osborne procedure; solid line: KERD resulting from the decomposition of the signal in the ion kinetic energy spectrum into two Gaussian functions. Bottom: contributions to the KERD from each Gaussian component (1 and 2) as well as their sum (1+2).

is characterized by $\langle T \rangle = 0.56$ eV, corresponding to an internal energy of 7.8 eV. The intensity ratio between the first and the second process is equal to 0.48. It must be stressed that this analysis assumes that the internal energy distribution consists only of two values, i.e. $E_{int} = 6$ eV and 7.8 eV. It is clear that the actual distribution is a continuous one: nevertheless, the satisfactory agreement between the KERD curves obtained by the Holmes–Osborne method and by the decomposition into two Gaussian components shows that the internal energy distribution is most probably characterized by two maxima located around the above-mentioned E_{int} values. The data for the other target gases are similar and are collected in table 3. One observes that the contribution of the second process decreases, as expected on the basis of our other data discussed in the previous sections, in the sequence: He > Ar > C_6H_6 > Xe.

The KER domain reached in our experiments (< 2 eV) can thus be accounted for by the model developed by Powis who considered the rotational predissociation of the electronic ground state NH_3^+ $\tilde{X}\,^2A_2''$ correlating directly to the NH_2^+ $(\tilde{X}\,^3B_1) + H(^2S)$ fragments [15,16]. Higher electronic states could also be involved in the loss of H. They could lead directly to electronically excited NH_2^+ (in its $\tilde{a}\,^1A_1$ or $\tilde{b}\,^1B_1$ states, e.g.) or to ground state NH_2^+ following internal or intersystem conversion (see fig. 1). Excited states have been detected by Locht et al. [18] by translational energy spectroscopy of fragment ions using a retarding potential method. For the NH_2^+ + H channel, they observe three structures in the KERD:

(i) an intense peak whose width at half height is equal to 1.4 eV; this corresponds to the entire KER domain sampled in our CAD experiments;

(ii) a shoulder at $T = 3.7$ eV, whose onset is located at an electron energy larger than 30 eV (internal energy > 20 eV);

(iii) a second peak at $T = 6.5$ eV appearing at an electron energy of 21.2 eV (internal energy = 11.1 eV).

Neither the shoulder nor the second peak appear in our KERD data. This means that the internal energy sampled under our experimental CAD conditions is certainly lower than 11 eV. This is consistent with the average internal energies obtained from the daughter ion spectra in a previous subsection. Let us also mention that the average KER values given in table 2 follow the same trend as the internal energies given in table 1.

Our data concerning the $NH_3^+ \rightarrow NH^+ + [H, H]$ channel (fig. 4) are consistent with the dissociative electroionization data of Syage [11] and of Locht et

Table 3
Decomposition of the kinetic energy release distribution for the $NH_3^+ \rightarrow NH_2^+ + H$ CAD process. $\langle T_1 \rangle$ and $\langle T_2 \rangle$ are the average kinetic energy releases associated with the two Gaussian components of the dissociation peak observed in the ion kinetic energy spectrum. T values are in eV

Target gas	$\langle T_1 \rangle$	$\langle T_2 \rangle$	Intensity ratio I_1/I_2	$\langle T \rangle$
He	0.13	0.56	0.48	0.42
Ar	0.11	0.53	0.50	0.39
Xe	0.08	0.44	0.99	0.26
C_6H_6	0.12	0.60	0.74	0.40

al. [18]. In particular, the $\langle T \rangle$ value measured by Syage (1.87 eV) is very close to our own results with He as the target gas (table 2 and fig. 4). In this case also, we observe two regimes in the KERD curves. Locht et al. observed that the kinetic energy release distribution of NH^+ resulting from dissociative electroionization broadens regularly as the electron energy is increased. Different onsets have been measured by these authors. Only the lowest ones will be relevant here. Besides the already mentioned onsets at 17 and 18 eV, a sharp increase in the appearance energy curves is detected at 22.6 eV. The next onset corresponds to the NH_3^+ ($\tilde{B}\,^2A_1$) state at 24.4 eV. They observed that T values in the 0–1.5 eV range are associated with the 18 eV onset whereas regularly increasing T values (1.5–7 eV) are observed starting from the appearance energy of 22.6 eV. Based on this work [18] we can propose the following interpretation of our KERD data.

(i) The first part of the KERDs, up to approximately 1.2 eV, results from dissociations occurring at or near the thermodynamical threshold. This process takes place directly from the $\tilde{A}$ state and leads to ground state fragments $NH^+(X\,^2\Pi) + H_2(X\,^1\Sigma_g^+)$.

(ii) The high energy part of the KERDs results from dissociations of NH_3^+ ions characterized by large internal energies allowing mainly the excitation of the $\tilde{B}\,^2A_1$ state of NH_3^+. Dissociation from this state can lead to electronic excitation of NH^+ (to the $A\,^2\Sigma^-$, $B\,^2\Delta$ or $C\,^2\Sigma^+$ states) and/or dissociation of H_2.

5. Conclusions

In this work, we have investigated several aspects of the collisionally activated decomposition of ammonia cations: the amount of energy transferred upon collision, the influence of the vibrational excitation of NH_3^+ on the collision and dissociation dynamics and the redistribution of the excess energy between the relative translational energy of the fragments (KER) and the internal degrees of freedom of these fragments.

Based on the branching ratios determined from daughter ion spectra, average internal energy values have been calculated and correlated to the nature of the target gas and to the collision energy. Benzene turns out to be a harder target than expected on the basis of its ionization energy: other parameters like the polarizability, the molecular field anisotropy and, especially, the excitation of internal degrees of freedom of the target must play a significant role. Excitation of the benzene target was indeed shown to be significant in the single electron capture by the ammonia dication [40].

With soft targets like Xe, we have shown that the CAD cross section increases with the amount of vibrational energy of the NH_3^+ projectile, giving insight into the electron impact ionization process. This vibrational excitation results from a nonadiabatic internal conversion between the $\tilde{A}$ and the $\tilde{X}$ state via a conical intersection [26]. Excitation of the projectile prior to collision also plays a role with the much harder He target as far as energy demanding processes like the loss of [H, H] are concerned.

The analysis of the kinetic energy release distributions shows a bimodal behaviour for both the loss of H and the loss of [H, H]. In the case of the H loss, collisionally activated dissociation takes place from the ground electronic state via rotational predissociation. Our data can be interpreted in the framework of the model developed by Powis [15,16]. On the other hand, for the loss of [H, H] the $\tilde{B}\,^2A_1$ excited state of NH_3^+ plays a significant role. Electronic excitation of NH^+ and/or dissociation of H_2 take place and the kinetic energy release distribution extends up to 7 eV.

Acknowledgement

We are indebted to Professor J. Momigny and Dr. R. Locht for interesting discussions and to Mr. P. Mélon for his invaluable help. We are particularly grateful to the Fonds de la Recherche Fondamentale Collective (Belgium), to the Belgian National Lottery, to the Communauté Française de Belgique and to the University of Liège for their generous financial support. BL thanks the Fonds National de la Recherche Scientifique (Belgium) for a research associate position.

References

[1] F.W. McLafferty, ed., Tandem mass spectrometry (Wiley–Interscience, New York, 1983).

[2] K.L. Busch, G.L. Glish and S.A. McLuckey, Mass spectrometry/mass spectrometry (VCH, Weinheim, 1988).
[3] G. Sahlström and I. Szabo, Arkiv Fysik 38 (1967) 145.
[4] E. v. Puttkamer, Z. Naturforsch. 25a (1970) 1062.
[5] J.D. Morrison and J.C. Traeger, Intern. J. Mass Spectrom. Ion Processes 11 (1973) 277.
[6] T.D. Märk, F. Egger and M. Cheret, J. Chem. Phys. 67 (1977) 3795.
[7] S.P. Khare and W.J. Meath, J. Phys. B 20 (1987) 2101.
[8] S.P. Khare, S. Prakash and W.J. Meath, Intern. J. Mass Spectrom. Ion Processes 88 (1989) 299.
[9] U. Müller and G. Schulz, Chem. Phys. Letters 170 (1990) 401.
[10] U. Müller and G. Schulz, J. Chem. Phys. 96 (1992) 5924.
[11] J.A. Syage, J. Chem. Phys. 97 (1992) 6085.
[12] J.A.R. Samson, G.N. Haddad and L.D. Kilcoyne, J. Chem. Phys. 87 (1987) 6416.
[13] G. Dujardin and S. Leach, Can. J. Chem. 63 (1985) 1386.
[14] M.F. Jarrold, A.J. Illies and M.T. Bowers, Chem. Phys. Letters 92 (1982) 653.
[15] I. Powis, J. Chem. Soc. Faraday Trans. II 77 (1981) 1433.
[16] I. Powis, Chem. Phys. 68 (1982) 251.
[17] R. Rüede, H. Troxler, Ch. Beglinger and M. Jungen, Chem. Phys. Letters 203 (1993) 477.
[18] R. Locht, Ch. Servais, M. Ligot, Fr. Derwa and J. Momigny, Chem. Phys. 123 (1988) 443.
[19] R. Locht, Ch. Servais, M. Ligot, M. Davister and J. Momigny, Chem. Phys. 125 (1988) 425.
[20] R. Locht and J. Momigny, Chem. Phys. 127 (1988) 435.
[21] P.A.M. van Koppen, A.J. Illies, S. Liu and M.T. Bowers, Org. Mass Spectrom. 17 (1982) 399.
[22] N. Kosugi, T. Ohta and H. Kuroda, Chem. Phys. 50 (1980) 373.
[23] A.R. Rossi and P. Avouris, J. Chem. Phys. 79 (1983) 3413.
[24] D. Power, P. Brint and T.R. Spalding, J. Molec. Struct. THEOCHEM 110 (1984) 155.
[25] S.A. Pope, I.H. Hillier and M.F. Guest, Faraday Symp. Chem. Soc. 19 (1984) 109.
[26] C. Krier, M.-Th. Praet and J.C. Lorquet, J. Chem. Phys. 82 (1985) 4073.
[27] I. Carmichael, Chem. Phys. 116 (1987) 351.
[28] P. Botschwina, J. Chem. Soc. Faraday Trans. II 84 (1988) 1263.
[29] W.P. Kraemer and V. Spirko, J. Mol. Spectry. 153 (1992) 276.
[30] R.K. Boyd and J.H. Beynon, Org. Mass Spectrom. 12 (1977) 163.
[31] M. Barber and R.M. Eliott, 12th Annual Conference on Mass Spectrometry and Allied Topics, Montreal, 1964, ASTM Committee E-14.
[32] H. Wankenne and J. Momigny, Intern. J. Mass Spectrom. Ion Phys. 7 (1971) 227.
[33] J.H. Beynon, R.G. Cooks, K.R. Jennings and A.J. Ferrer-Correia, Intern. J. Mass Spectrom. Ion Phys. 18 (1975) 87.
[34] P.J. Todd and F.W. McLafferty, Intern. J. Mass Spectrom. Ion Phys. 38 (1981) 371.
[35] J.L. Holmes, Org. Mass Spectrom. 20 (1985) 169.
[36] J.L. Holmes and A.D. Osborne, Intern. J. Mass Spectrom. Ion Phys. 23 (1977) 189.
[37] B.J. Kim and M.S. Kim, Intern. J. Mass Spectrom. Ion Processes 98 (1990) 193.
[38] B. Leyh and H. Wankenne, Intern. J. Mass Spectrom. Ion Processes 107 (1991) 453.
[39] M.S. Kim and F.W. McLafferty, J. Am. Chem. Soc. 100 (1978) 3279.
[40] B. Leyh and A. Hoxha, to be published.
[41] G. Mauclaire, M. Heninger, S. Feinstein, J. Wronka and R. Marx, Intern. J. Mass Spectrom. Ion Processes 80 (1987) 99.